Magnetoelastic and thermal effects in the BiMn$_2$O$_5$ lattice: A high-resolution x-ray diffraction study

E. Granado,[1,2,][*] M. S. Eleotério,[1,2] A. F. García-Flores,[1] J. A. Souza,[3] E. I. Golovenchits,[4] and V. A. Sanina[4]

[1]*Instituto de Física "Gleb Wataghin," UNICAMP, Caixa Postal 6165, 13083-970, Campinas, São Paulo, Brazil*
[2]*Laboratório Nacional de Luz Síncrotron, Caixa Postal 6192, 13084-971, Campinas, São Poulo, Brazil*
[3]*Instituto de Física, Universidade de São Paulo, Caixa Postal 66318, 05315-970, São Paulo, Brazil*
[4]*Ioffe Physical-Technical Institute of RAS, 194021 St. Petersburg, Russia*

High-resolution synchrotron x-ray diffraction measurements were performed on single crystalline and powder samples of BiMn$_2$O$_5$. A linear temperature dependence of the unit cell volume was found between T_N = 38 and 100 K, suggesting that a low-energy lattice excitation may be responsible for the lattice expansion in this temperature range. Between $T^* \sim 65$ K and T_N, all lattice parameters showed incipient magnetoelastic effects, due to short-range spin correlations. An anisotropic strain along the **a** direction was also observed below T^*. Below T_N, a relatively large contraction of the a parameter following the square of the average sublattice magnetization of Mn was found, indicating that a second-order spin Hamiltonian accounts for the magnetic interactions along this direction. On the other hand, the more complex behaviors found for b and c suggest additional magnetic transitions below T_N and perhaps higher-order terms in the spin Hamiltonian. Polycrystalline samples grown by distinct routes and with nearly homogeneous crystal structure above T_N presented structural phase coexistence below T_N, indicating a close competition amongst distinct magnetostructural states in this compound.

I. INTRODUCTION

Multiferroic materials with coexisting (anti)ferromagnetism and ferroelectricity have attracted renewed attention, due to the interesting physics involved as well as relevant potential applications in spintronics. A fairly strong coupling amongst ferroelectric and magnetic order parameters may occur as a result of exchange striction effects in magnetic structures lacking an inversion center (for a recent review, see Ref. [1]). Examples can be found within the class of frustrated antiferromagnets. The RMn$_2$O$_5$ family is a particularly interesting case,[2,3] in which Mn^{4+}O$_6$ octahedra and Mn^{3+}O$_5$ pyramids are interconnected and no possible spin configuration can simultaneously satisfy all nearest-neighbor Mn-O-Mn superexchange interactions.[4–6] As a consequence, the magnetic structures actually found in this family frustrates some of the spin interactions. Below the magnetic ordering temperature, slight atomic displacements take place and strengthen (weaken) the satisfied (frustrated) interactions, breaking the inversion symmetry of the structure and leading to ferroelectricity.[4–7]

While the above mechanism explains qualitatively the multiferroic behavior of RMn$_2$O$_5$, detailed experimental information on the atomic displacements associated with each of the commensurate or incommensurate spin structures of this family is still lacking. This is mostly due to the small magnitude of such displacements, presumably below ~ 0.01 Å.[7] This limitation prevents a more quantitative test for the existing theories, most noticeably for *ab initio* calculations.[7] On the other hand, the lattice parameters can be obtained directly by high-resolution x-ray diffraction experiments, and the thermal expansion coefficients may be also accurately obtained by macroscopic dilatometry measurements on single crystals. Such measurements may reveal

the overall magnetoelastic coupling in the unit cell dimensions, and carry relevant information on the microscopic spin-lattice coupling mechanism leading to ferroelectricity. Dilatometry measurements of thermal expansion coefficients have been carried out for R=Ho, Dy, and Tb,[8] clearly revealing the lattice anomalies related to each of the magnetic transitions of these materials.

It is well known that thermal expansion coefficients obtained by macroscopic dilatometry may have much higher resolution than the typical results of x-ray or neutron diffraction. On the other hand, diffraction is the only choice to investigate powder samples with anisotropic crystal structure, and may be also useful for single crystal studies if simultaneous lattice expansion and strain broadening measurements are required. This is generally the case in investigations of ferroelectric materials,[9] which commonly have distinct behaviors for powder and single crystalline samples, also depending on the details of sample growth. Thus, a technique combining the attributes of high resolution to detect minute lattice anomalies and microscopic sensitivity to probe powder samples and/or inhomogeneous phases is highly desirable to study ferroelectric materials, in particular, the multiferroics. In fact, high-resolution synchrotron x-ray diffraction may be the technique of choice for some of these cases.

BiMn$_2$O$_5$ presents a magnetic structure with propagation vector $\tau = (1/2, 0, 1/2)$ at low temperatures,[10,11] while other members show ground states with $\tau = (k_x, 0, k_z)$ with $k_x \sim 1/2$ and $0.25 \leqslant k_z \leqslant 0.37$.[4–6,12–14] Structurally, the major differences to the other compounds of the series arise from a largely distorted BiO$_8$ cage, which has been ascribed to the electron lone pair in Bi^{3+}.[11] No detailed study on the magnetoelastic properties of this compound has been performed, to our knowledge. To bridge this gap, we performed a synchro-

tron x-ray diffraction study on a single crystal of $BiMn_2O_5$, as well as on two powder samples grown by distinct routes. It is shown that this technique may have enough resolution to reveal the relatively subtle lattice parameter anomalies related to the magnetic transitions and may provide quantitative details of the spin-lattice coupling in this compound.

II. EXPERIMENTAL DETAILS

The single crystal used in the present study was prepared by the flux method, as described elsewhere.[3,15] In addition, two polycrystalline samples of $BiMn_2O_5$ (BMO) were grown by entirely different routes. The sample named BMO1 was grown by wet chemistry[16] using the procedure described in Ref. [11], while BMO2 was grown by a solid state reaction: stoichiometric amounts of Bi_2O_3 and Mn_2O_3 were thoroughly mixed in an agate mortar, and heated to 800 °C for 48 h and to 900 °C for 72 h, with intermediate grindings at each 24 h. For powder diffraction experiments, a sieve was used to reject grains larger than ∼5 μm, and the samples were deposited over flat Cu holders, apropriate for Bragg-Brentano geometry. Synchrotron x-ray diffraction experiments in the single crystal and powder samples were performed on the XPD beamline of the Laboratório Nacional de Luz Síncrotron (LNLS),[17] using an incident beam with λ =1.5499 Å for the single crystal study and λ=1.3773 Å for the powder measurements, except when otherwise stated. The beam was focused onto a spot ∼0.8×2.0 mm^2 for the single crystal and ∼0.8×5.0 mm^2 for powders at the sample position. A Ge(111) analyzer crystal was placed in a goniometer attached to the 2θ arm, and a scintillation detector was used. The instrumental resolution for this setup was ∼0.01° full width at half maximum (FWHM) at 2θ=25°,[17] and a step width of 0.0025° was chosen for the powder measurements while the sample was rocked by 1° during each observation to minimize graininess effects. For single crystal measurements, a natural (001) surface with no treatment was chosen, and the lattice parameters were obtained from the Bragg positions of the (402), (045), and (006) reflections. Each reflection showed a clearly split three-peak structure in the axial $(\theta-2\theta)$ scans at all temperatures, indicating the presence of at least three domains with distinct sets of lattice parameters, possibly due to inhomogenously distributed Bi vacancies. All the domains showed identical temperature dependence for the lattice parameters, and the results shown in this work (including the peak widths) are given for the strongest peak of each Bragg reflection. A closed cycle He cryostat was employed in our measurements, and the temperature was measured with an estimated accuracy better than ∼1 K and stability of ∼1 mK. All the measurements were performed below ∼100 K, while the base temperature (11 K for powders and 17 K for the single crystal) was determined by the performance of the cryostat at the time of the experiments. dc-magnetic susceptibility measurements were performed on a commercial superconduction quantum interference device (SQUID) magnetometer, while the specific heat was measured on a commercial platform using the relaxation method.
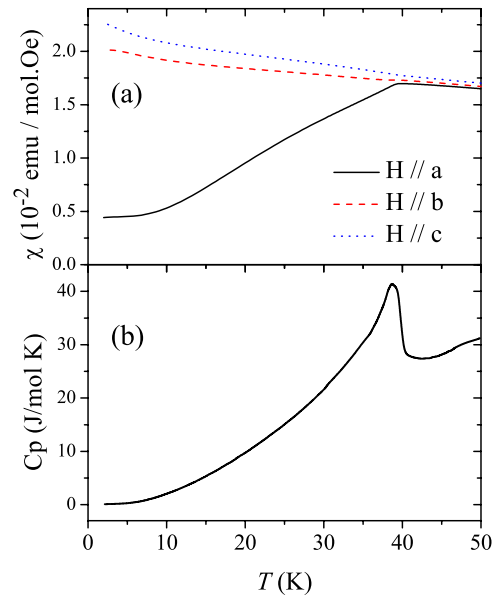

FIG. 1. (Color online) Temperature dependence of (a) magnetic susceptibility taken with a magnetic field of 2000 Oe along the **a**, **b**, and **c** directions; and (b) specific heat of the $BiMn_2O_5$ single crystal.

III. RESULTS AND ANALYSIS

A. dc-magnetic susceptibility and specific heat

$BiMn_2O_5$ has been described as a noncolinear commensurate antiferromagnet at low temperatures with propagation vector $\vec{\tau}=(\frac{1}{2},0,\frac{1}{2})$, and the spins pointing nearly along the **a** direction, as inferred from neutron powder diffraction (NPD) measurements by Muñoz *al.*[11] As a preliminary bulk characterization, we performed dc-magnetic susceptibility (χ_{dc}) and specific heat (C_p) measurements on the single crystal [see Figs. 1(a) and 1(b)]. Only one transition could be unequivocally distinguished in our C_p data, within our resolution, while χ_{dc} data show that the Mn spins are indeed oriented nearly along the **a**-direction in the ordered phase, as inferred by the smaller susceptibility below T_N with the field along this direction. The χ_{dc} data are consistent to those reported in Ref. [18], and the conclusions drawn from χ_{dc} and C_p data are entirely consistent with the previous NPD results.[11] (χ_{dc}) measurements on the two powder samples also confirmed the antiferromagnetic (AFM) transition at $T_N \sim 38-40$ K.

B. X-ray diffraction

Figures 2(a)–2(c) show the temperature dependence of the a, b, and c lattice parameters obtained from the single crystal. The corresponding unit cell volume V is given in Fig. 2(d). For temperatures between ∼T^*=65 and 100 K (our upper limit in this work), the evolution of all the lattice parameters follows a straight line within our resolution. The linear thermal expansion coefficients in this T range are $\alpha_a =(1/a)\delta a/\delta T=7.7(1)\times10^{-6}$ K^{-1}, $\alpha_b=1.7(2)\times10^{-6}$ K^{-1}, and $\alpha_c=3.27(4)\times10^{-6}$ K^{-1}; and the volumetric expansion coefficient is $\beta=1.27(3)\times10^{-5}$ K^{-1}. For $T_N<T\lesssim T^*$, deviations from this behavior were observed. Interestingly, such
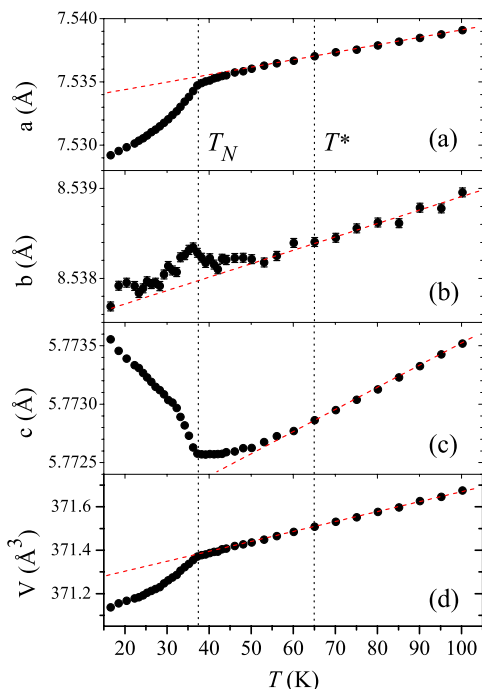
FIG. 2. (Color online) Temperature dependence of the a, b, and c lattice parameters, and unit cell volume V for the single crystal. The dashed lines fitting the data above 65 K are guides to the eyes. The vertical lines mark the magnetic ordering temperature T_N and the onset of the strongly correlated paramagnetic state (see text and Ref. 21). Except in (b), statistical error bars are smaller than the symbol size.

deviations had a distinct sign for the a lattice parameter with respect to b and c, so that the unit cell volume followed the constant thermal expansion down to $T_N \sim 38$ K. At T_N, clear anomalies were observed for all lattice parameters and unit cell volume. While the a lattice parameter shows a contraction below T_N, the b parameter shows a peaklike feature close to T_N and c shows an expansion on cooling. The dominant contraction of a shown in Fig. 2(a) leads to a significant reduction of the unit cell volume below T_N [see Fig. 2(d)].

In order to correlate the observed lattice parameter anomalies to the antiferromagnetic order parameter and obtain more detailed information on the magnetoelastic coupling in this material, the contributions from the nonmagnetic thermal expansion coefficient were subtracted, leading to magnetoelastic contributions to a, b, and c, which we refer to as a_M, b_M, and c_M [see Fig. 3(a)]. For this procedure, we assumed that the nonmagnetic contributions to the lattice expansion have linear temperature dependence also below T_N, at least down to 17 K. These data were compared to the square of the average sublattice magnetization of the Mn^{4+} ($4f$ site) and Mn^{3+} ($4h$ site) ions (M^2), extracted from Ref. 11 also normalized at 17 K [see Fig. 3(b)]. It is interesting to note that the evolution of a_M closely follows M^2 below T_N. The peaklike feature in the b_M parameter takes place at ~ 36 K, clearly below T_N, while c_M appears to show a feature at ~ 33 K, increasing linearly on further cooling (see Fig. 2).

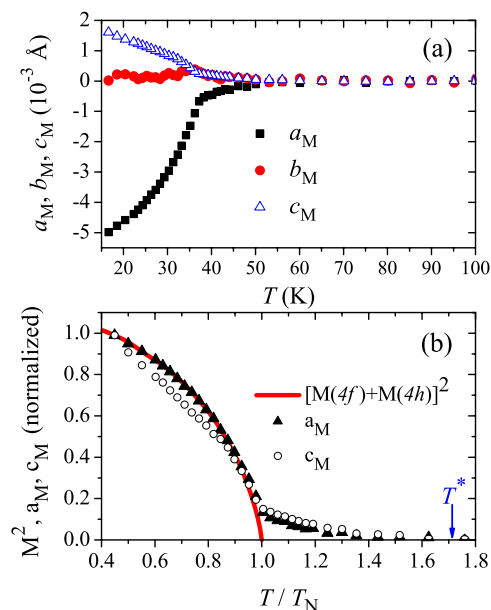Figure 4 shows the width of the (402) and (045) reflec-

FIG. 3. (Color online) (a) Magnetoelastic component of a, b, and c lattice parameters, defined as the difference between the symbols and straight line in Fig. 2 and labeled as a_M, b_M, and c_M, respectively. (b) Scaling of a_M and c_M, normalized at 17 K (symbols), with the squared average sublattice magnetization of Mn^{4+} and Mn^{3+} ions (solid line), extracted from Ref. 11. Statistical error bars are smaller than the symbol size.

tions, revealing a broadening of (402) on cooling below T^* and a nearly constant width of (045). Such anisotropic strain broadening indicates a magnetically driven fluctuation of the a lattice parameter throughout the sample, in contrast to b and c, which did not show temperature dependent strain broadening, within the precision of our experiment.

Figure 5(a) shows the full powder diffraction pattern of BMO2 at 100 K. The crystal structure was refined under the *Pbam* space group using the GSAS+EXPGUI suite.[19,20] The structure reported in Ref. 11 at 300 K was used as the initial model for the refinement. The calculated profile after the refinement is also shown in Fig. 5. The experimental data
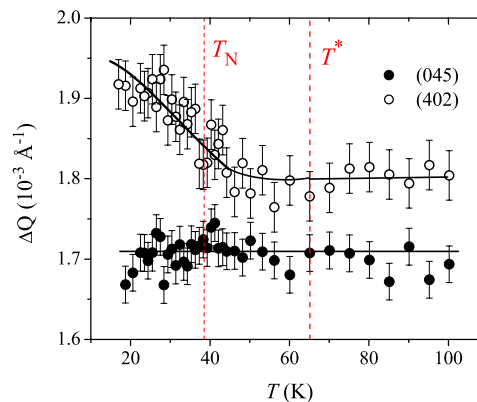

FIG. 4. (Color online) Bragg peak widths obtained from radial ($\theta - 2\theta$) scans around the (402) and (045) reflections for the single crystal. The solid lines are guides to the eyes.
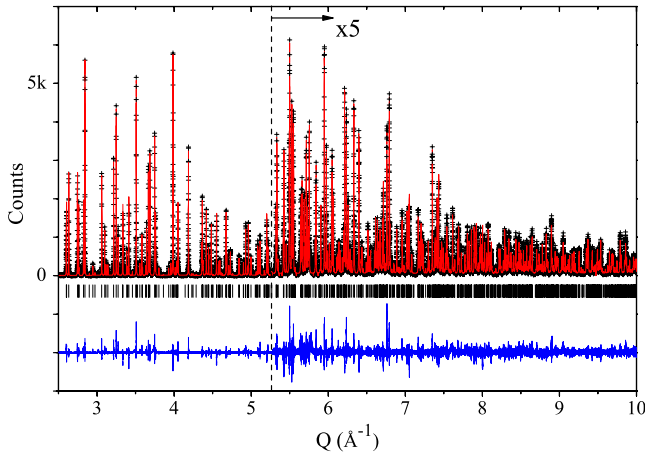
FIG. 5. (Color online) (a) Observed (symbols), calculated (line), and difference (botton line) x-ray powder diffraction profile of sample BMO2 at 100 K, taken with $\lambda = 1.1271$ Å. The goodness-of-fit factors are $R_p = 13.6\%$ and $R_p = 24.9\%$ (background subtracted), and $\chi^2 = 1.85$. The data were multiplied by 5 above $Q = 5.3$ Å^{-1} for better visualization. The experimental data with $Q < 2.5$ Å^{-1} were excluded from the refinement (see text).

with $Q < 2.5$ Å^{-1} were excluded from this refinement to avoid the instrumental or extrinsic effects of peak asymmetry, self-absorption due to surface roughness, and beam footprint larger than the sample size, which become noticeable at lower angles for the reflection geometry employed here. This procedure does not affect significantly the accuracy and precision of the refined parameters, since the density of Bragg peaks is larger in the higher Q region. The overall fitting quality is satisfactory, and the refined structural parameters are given in Table I. The relevant interatomic distances are given in Table II. No impurity phases were observed within our sensitivity. A similar structural refinement was attempted for BMO1 and was unsuccessful, due to more severe expurious intensity fluctuations in each Bragg peak associated with graininess. Paradoxically, this technical problem arises due to a better cristallinity (sharper Bragg peaks) of BMO1, making it less probable for an individual grain to satisfy the Bragg condition and reducing the number of crystallites simmultaneously contributing to each peak. We should mention

that BMO1 also revealed weak unidentified impurity peaks ($<0.5\%$ of the strongest peak of the main phase). Overall, both samples were found to be homogeneous and of very good crystalline quality above T_N. No sign of anisotropic strain or symmetry lowering was observed for both samples at 100 K.

Figures 6(a) and 6(b) show a selected portion of the powder diffraction profiles for BMO1 and BMO2, respectively, including the (210) and (021) Bragg peaks, at several temperatures. It can be observed that, while the (021) peak shows nearly no T dependence, the (210) reflection splits into two peaks at low T. A similar splitting was clearly identified in many other (hkl) reflections with a large $h/(k+l)$ ratio. Attempts to index all Bragg peaks at 10 K within a single crystallographic phase with either a monoclinic or triclinic unit cell derived from the high-temperature orthorhombic cell were unsuccessfull. On the other hand, a model with two distinct phases with *Pbam* symmetry and slightly different sets of lattice parameters could match the observed Bragg peak splittings in the powder profile. These phases were labeled as P1 and P2 in Figs. 6(a) and 6(b). In order to avoid divergences in the fit, the b lattice parameter had to be constrained as equal in both phases. The refined lattice parameters for P1 and P2 at 10 K are given in Table III. It can be seen that P1 has smaller a and slightly larger c than P2. Unfortunately, the atomic parameters of P1 and P2 at 10 K could not be reliably extracted from the refinement, since the fit did not converge when all the relevant atomic parameters were simultaneously refined. This is mostly likely due to significant Bragg peak overlap of the two coexisting phases.

To gain further insight into the nature of phases P1 and P2 below T_N, the Bragg peak positions of the (210) reflections of both phases, obtained from a fit with Lorentzian line shapes (symbols), are given in Fig. 7(a) for samples BMO1 and BMO2. For temperatures above T_N, the positions of the single (210) peak corresponding to the unique structural phase are given. For the temperature interval near and below T_N in which the two peaks could not be reliably separated in the fit, the positions are not given in this figure. The "expected" positions of the (210) reflections, obtained from the single crystal data of Figs. 2(a)–2(c), are given in Fig. 7(a) (solid line). An analysis of the (210) and (021) peaks widths obtained with a single Lorentzian fit for each reflection is

TABLE I. Refined lattice and atomic parameters of sample BMO2 at 100 K. Errors in parentheses are statistical only, and represent one standard deviation.

$T = 100$ K		*Pbam*	$a = 7.54116(1)$ Å	$b = 8.52994(1)$ Å	$c = 5.75437(1)$ Å	
Atom	Site	x	y	z	U_{iso} (Å^2)	Frac
Bi	$4g$	0.15896(4)	0.16556(4)	0	0.00588(6)	0.938(4)
Mn1	$4f$	1/2	0	0.2596(2)	0.0021(2)	1
Mn2	4 h	0.40755(15)	0.35091(14)	1/2	0.0029(2)	1
O1	$4e$	0	0	0.2876(10)	0.0048(5)	1
O2	$4g$	0.1567(8)	0.4453(6)	0	0.0048(5)	1
O3	4 h	0.1437(7)	0.4243(6)	1/2	0.0048(5)	1
O4	$8i$	0.3866(5)	0.2018(4)	0.2525(7)	0.0048(5)	1
$R_p = 13.6\%$			$R_{wp} = 25.3\%$			$\chi^2 = 1.86$

TABLE II. Interatomic distances for sample BMO2 at 100 K (Å). Errors in parentheses are statistical only, and represent one standard deviation.

	$Mn^{4+}O_6$		
Mn1-O2(×2)	1.961(4)		
Mn1-O3(×2)	1.872(4)		
Mn1-O4(×2)	1.923(4)		
⟨Mn1-O⟩	1.919(2)		
	$Mn^{3+}O_5$		
Mn2-O1(×2)	1.897(4)		
Mn2-O3(×1)	2.086(6)		
Mn2-O4(×2)	1.916(4)		
⟨Mn2-O⟩	1.966(3)		
		BiO_8	
Bi-O1(×2)	2.484(4)		
Bi-O2(×1)	2.337(5)	Bi-O2(×1)	2.386(5)
Bi-O4(×2)	2.270(4)	Bi-O4(×2)	2.758(4)
⟨Bi-O⟩	2.468(2)		

given in Fig. 7(b). While the (021) width shows only a weak temperature dependence, the (210) width increases steeply for temperatures below $\sim T_N$, for both BMO1 and BMO2 samples. This result shows that the onset of structural phase coexistence on powder samples takes place near the magnetic ordering temperature, $T_N \sim 38–40$ K.

IV. DISCUSSION

We begin our discussion by considering the lattice parameter behavior above T_N (see Fig. 2). In this temperature region, the thermal expansion is highly anisotropic, α_a being much larger than α_b and α_c. Remarkably, the unit cell volume V shows a linear temperature dependence between $\sim T_N$ and 100 K within our resolution, indicating a nearly constant thermal expansion coefficient β. This is a highly unusual behavior, since $\beta = b_3 T^3 + b_5 T^5 + b_7 T^7 + \cdots$ is expected at sufficiently low temperatures,[22] and a constant β should occur only for $T \gg \theta_D$, where $\theta_D = 235$ K is the Debye temperature for $BiMn_2O_5$.[11] A possible explanation for this intriguing behavior is the hypothetical presence of a very low-frequency optical mode or some other dispersionless lattice excitation, which thermal population might dominate the lattice expansion below 100 K. This possible mode or excitation might be associated with coupled rigid rotations of the MnO_6 octahe-

dra and MnO_5 pyramids, or most likely be a rattling motion of Bi ions inside the BiO_8 cage. We should mention that an anomalous distribution of Tb-O distances was observed for the related compound $TbMn_2O_5$, with relatively large thermal dependence even at low temperatures,[24] also suggesting low-energy lattice excitations in this family. Considering the linear volumetric thermal expansion above T_N, we expect that the energy of such mode should satisfy the relation $E \ll k_B T_N = 3.4$ meV. Preliminary Raman[25] and infrared[26] spectroscopy measurements did not reveal any clear optical phonon with energies between ~ 2 and ~ 5 meV, indicating that the suggested lattice excitation is either silent or has an energy below ~ 2 meV. We should mention that, since the linear temperature dependence of V occurs in the paramagnetic and/or paraelectric phase, it cannot be explained by the possible presence of electromagnons in the ferroelectric and/or antiferromagnetic phase.[27–30]

Even though the unit cell volume shows a linear temperature dependence down to T_N, the individual lattice parameters a, b, and c present deviations from a linear behavior below $T^* \sim 65$ K. The sign of this deviation for a is opposite to that for b and c [see Figs. 2(a)–2(c)], compensating each other in the volumetric expansion between T_N and T^*. Also, these relatively small deviations from the linear temperature dependence in the paramagnetic region have the same sign of the much larger magnetoelastic anomalies below T_N, i.e., a

TABLE III. Lattice parameters and unit cell volume for phases P1 and P2 of powder samples BMO1 and BMO2 at 10 K. Errors in parentheses are statistical only, and represent one standard deviation.

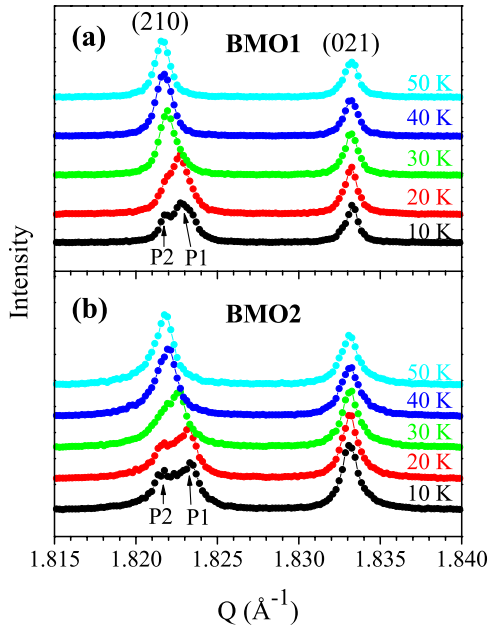| Sample	Phase	Fraction (%)	a (Å)	b (Å)	c (Å)	V (Å³)
BMO1	P1	90(2)	7.53039(3)	8.52766(3)	5.75426(3)	369.517(3)
BMO1	P2	10(2)	7.53730(7)	8.52766(3)	5.75377(10)	369.827(6)
BMO2	P1	53(1)	7.53094(3)	8.52955(3)	5.75497(3)	369.673(3)
BMO2	P2	47(1)	7.53888(4)	8.52955(3)	5.75405(3)	370.004(3)

FIG. 6. (Color online) (a) Small portion of the powder diffraction profile of BMO1 and BMO2 samples covering the (201) and (021) reflections at selected temperatures. The profiles were vertically translated for better visualization.
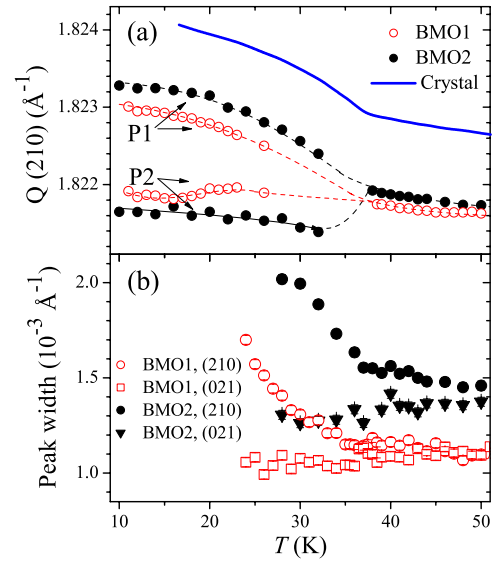

FIG. 7. (Color online) (a) Symbols: temperature dependence of the positions of the (210) reflection for P1 and P2 phases of BMO1 and BMO2 powder samples (see Fig. 6). The solid line indicates the expected behavior taken from single crystal data shown in Fig. 2. (b) Temperature dependence of the width of the (210) and (021) reflections of BMO1 and BMO2, taken in the temperature region where the scattering at the (210) position could be fitted by a single Lorentzian peak. Statistical error bars are smaller than the symbol size.

contraction for a and an expansion for b and c on cooling. This correspondence suggests that the deviations from linear temperature dependence between T_N and T^* are not driven by phonons, but are rather related to the strong short-range spin correlations in this temperature region, consistent with a previous Raman scattering study in $BiMn_2O_5$.[21] The magnetically driven strain broadening of the (402) reflection below $\sim T^*$ (see Fig. 4) is an additional evidence that short-range spin correlations may influence the crystal lattice of $BiMn_2O_5$.

The most noticeable lattice anomalies take place below T_N, deserving a careful consideration. In a quadratic spin Hamiltonian for transition-metal compounds, the magnetic energy and the atomic displacements due to exchange striction are proportional to the square of the magnetic order parameter (M^2), in a mean-field approximation, assuming that the angles between ordered spins remain constant below T_N. This proposition is valid for either Heisenberg, Ising, or Dzyaloshinskii-Moriya spin Hamiltonians, or a combination of them. In order to accomodate the atomic movements directly related to exchange striction, the crystal lattice relaxes, possibly leading to complex structural changes even for atoms not directly related to the exchange mechanism. For small displacements, the magnitude of the elastic response of the lattice is directly proportional to the perturbing displacements due to exchange striction; therefore, the overal lattice anomalies arising from exchange striction are expected to follow M^2 for a quadratic spin Hamiltonian. Figure 3(b) shows that this simple prediction is confirmed for a_M, but clearly fails for b_M and c_M in the whole studied temperature interval. In addition, these two parameters show interesting features at ~ 36 and ~ 33 K that might be associated with additional magnetic transitions below T_N. We speculate that

these anomalies might be due to spin-flip and/or incommensurate-commensurate magnetic transitions, such as observed in other members of the family.[8] We should mention that no evidence of multiple magnetic transitions has been observed in our C_p data, within our temperature resolution, while a two-peak structure in C_p close to T_N was previously reported.[11] More detailed neutron diffraction experiments in the temperature interval close to T_N may be necessary to confirm or dismiss this hypothesis.

The fact that only a_M scales with M^2 is interesting. This is also the direction in which the magnitude of the lattice anomaly is the largest. This can be rationalized on the basis of the magnetic structure of $BiMn_2O_5$ given in Ref. 11. According to this, along the **a**-direction all the nearest-neighbor spin alignment between $Mn^{4+}O_6$ octahedra and $Mn^{3+}O_5$ pyramids and between consecutive $Mn^{3+}O_5$ pyramids in the sequence $\cdots Mn^{4+}-Mn^{3+}-Mn^{3+}-Mn^{4+}\cdots$ are nearly AFM, with no clear manifestation of magnetic frustration except perhaps for a relatively small noncollinearity of the spin alignment. On the other hand, the spin alignment along **b** and **c** directions shows clear signs of competing interactions. Along **b**, the coupling between $Mn^{4+}O_6$ octahedra and $Mn^{3+}O_5$ pyramids alternates between ferromagnet (FM) and AFM, breaking the inversion symmetry of the structure and possibly causing ferroelectricity as in other members of the RMn_2O_5 family.[1] Along **c**, the spin aligment between edge-shared $Mn^{4+}O_6$ octahedra also alternates between FM and AFM, the AFM and FM alignments corresponding to the shorter ($=2.767$ Å) and longer ($=2.988$ Å) $Mn^{4+}-Mn^{4+}$ distances, respectively. Bi and Mn^{3+} planes are intercalated be-

tween the AFM- and FM-coupled Mn^{4+} planes, respectively. It has been argued that the $Mn^{4+}-O-Mn^{3+}-O-Mn^{4+}$ super-exchange path and the longer $Mn^{4+}-Mn^{4+}$ distances may help stabilizing the FM coupling among half of the Mn^{4+} pairs.[11] We mention that, while the Mn spin structures in the ab plane are similar for all members of the family, the alignment along **c** is strongly dependent on the R ions, with the component of the spin propagation vector varying from $k_z = 1/4$ for $R=$Er (Ref. [12]) to $k_z=1/2$ for $R=$Bi.[10,11] This is another clear indication of competing magnetic interactions along this direction.

The distinct features of the magnetic ordering along each direction obviously lead to an anisotropic magnetoelastic coupling, as manifested in the data of Fig. 2. First of all, the AFM alignment of nearest-neighbor spins along **a** leads to a relatively large contraction of the lattice along this direction below T_N [see Fig. 2(a)], in order to enhance the AFM coupling of the $\cdots Mn^{4+}-Mn^{3+}-Mn^{3+}-Mn^{4+}\cdots$ chains. On the other hand, some of the magnetic interactions are frustrated along **b**, and therefore the atomic distances related to "satisfied" pairs are expected to be reduced and others (between "frustrated" pairs) should increase below T_N, leading to a compensation which is manifested as small values of b_M in comparison to a_M (see Fig. 3). In the case of c_M, a presumed increase of the separation of FM Mn^{4+} pairs may be partially compensated by a corresponding approximation between the AFM Mn^{4+} pairs or vice versa, leading to smaller c_M anomalies in comparison to a_M. In addition, the evolution of b_M and c_M may be also influenced by a lattice relaxation in response to the relatively large contraction of a_M. Even considering such a complex situation, it is expected that magnetoelastic anomalies along all directions should follow the square of the sublattice magnetization for a spin Hamiltonian composed only of quadratic terms on spin, as argued above. The fact that c and most notably b do not follow this behavior even for the temperature interval where no additional phase transitions are evidenced ($T<33$ K) suggest that other terms, possibly of fourth order (biquadratic, three spin, and four spin),[23] should be included in the spin Hamiltonian to correctly account for the magnetoelastic anomalies in $BiMn_2O_5$. Although these terms are expected to be significantly smaller than the quadratic exchange terms, the magnetic frustration caused by the complex lattice geometry may cause a nearly complete cancellation of the quadratic terms, leading to a relative increase of the importance of the fourth-order terms, and consequently a manifestation of such terms in the magnetoelastic anomalies in the directions where the spin frustration is most pronounced. This conclusion is likely extensible to the other members of the RMn_2O_5 family and may be of relevance to a quantitative understanding of their complex magnetic phase diagram and multiferroic properties.

The analysis of the powder samples provides relevant additional information. Contrary to the single crystal, a coexistence of two distinct phases with orthorhombic metrics (within our resolution) and slightly different sets of a and c lattice parameters was observed below $\sim T_N$ for both BMO1 and BMO2 powder samples. The lattice parameters of P1 are closer to P2 in BMO1 than in BMO2, indicating that the magnitude of this effect in powder samples is dependent on the sample details. The phase fractions of P1 and P2 are also strongly sample dependent (see Table III). Also, a comparison of the T dependence of the position of a particular Bragg peak with temperature of both powder samples with that expected from single crystal data (see Fig. 7) shows that the phase labeled P1 (with smaller a lattice parameter) corresponds to the magnetostructural ground state of $BiMn_2O_5$, while P2 may be either a metastable state or phase stabilized by slight chemical inhomogeneities (see below). It is well known that powder samples may favor the presence of metastable structural phases not generally observed on single crystals, leading to polymorphism. In the present case, the structures of P1 and P2 converge above T_N, showing that the phase separation cannot be trivially explained by large chemical inhomogeneities between distinct grains. In fact, P2 presumably shows a different magnetic structure than P1, leading to distinct magnetoelastic coupling effects and therefore a slightly different set of lattice parameters at low temperatures. On the other hand, slight chemical inhomogeneities (such as in the Bi occupancy) not clearly evidenced in our powder diffraction profiles above T_N might still play a role in stabilizing a magnetically phase-separated state below T_N if there is a pre-existing close competition between distinct possible magnetic ground states. The fact that P1 and P2 unit cells show differences in a and c lattice parameters with no observable change in b suggests that magnetic structures of these phases show distinct components of the propagation vector along **a** and/or **c**. Further studies are necessary to confirm or dismiss this hypothesis.

V. CONCLUSIONS

In summary, the magnetoelastic anomalies in single crystal and powdered $BiMn_2O_5$ were investigated in detail by high-resolution synchrotron x-ray diffraction. It was found in the single crystal study that this compound shows a linear temperature dependence of the unit cell volume between T_N and 100 K, well below the Debye temperature, which has been associated with the possible presence of a low-energy lattice excitation that still remains to be directly observed. Below T_N, significant lattice parameter anomalies were found, most notably in the a parameter, due to a magnetoelastic coupling. The anomaly of a was found to follow the square of the average sublattice magnetization, as expected for a quadratic spin Hamiltonian. The anomalies of b and c follow a more complex behavior, signaling the existence of additional transitions below T_N as in other members of the RMn_2O_5 family, and perhaps higher-order terms in the spin Hamiltonian. It was argued that strong short-range spin correlations between T_N and $T^*=65$ K (Ref. [21]) give rise to an observable contribution to the linear thermal expansion coefficients. X-ray powder diffraction measurements taken on samples grown by distinct routes show phase coexistence of different magnetostructural states below T_N. One of these states corresponds to that observed in the single crystal, while the other was attributed to a competing magnetic state which might be metastable or stabilized by subtle chemical inhomogeneities that might be present in the powder samples.

*egranado@ifi.unicamp.br

[1] S.-W. Cheong and M. Mostovoy, Nature (London) **6**, 13 (2007).

[2] N. Hur, S. Park, P. A. Sharma, J. S. Ahn, S. Guha, and S.-W. Cheong, Nature (London) **429**, 392 (2004).

[3] N. Hur, S. Park, P. A. Sharma, S. Guha, and S.-W. Cheong, Phys. Rev. Lett. **93**, 107207 (2004).

[4] L. C. Chapon, G. R. Blake, M. J. Gutmann, S. Park, N. Hur, P. G. Radaelli, and S.-W. Cheong, Phys. Rev. Lett. **93**, 177402 (2004).

[5] G. R. Blake, L. C. Chapon, P. G. Radaelli, S. Park, N. Hur, S.-W. Cheong, and J. Rodríguez-Carvajal, Phys. Rev. B **71**, 214402 (2005).

[6] L. C. Chapon, P. G. Radaelli, G. R. Blake, S. Park, and S.-W. Cheong, Phys. Rev. Lett. **96**, 097601 (2006).

[7] C. Wang, G.-C. Guo, and L. He, Phys. Rev. Lett. **99**, 177202 (2007).

[8] C. R. dela Cruz, F. Yen, B. Lorenz, M. M. Gospodinov, C. W. Chu, W. Ratcliff, J. W. Lynn, S. Park, and S.-W. Cheong, Phys. Rev. B **73**, 100406(R) (2006).

[9] M. Mir, V. R. Mastelaro, P. P. Neves, A. C. Doriguetto, D. Garcia, M. H. Lente, J. A. Eiras, and Y. P. Mascarenhas, Acta Crystallogr., Sect. B: Struct. Sci. **63**, 713 (2007).

[10] E. F. Bertaut, G. Buisson, S. Quezel-Ambrunaz, and G. Quezel, Solid State Commun. **5**, 25 (1967).

[11] A. Muñoz, J. A. Alonso, M. T. Casais, M. J. Martínez-Lope, J. L. Martínez, and M. T. Fernández-Diaz, Phys. Rev. B **65**, 144423 (2002).

[12] G. Buisson, Phys. Status Solidi A **16**, 533 (1973); **17**, 191 (1973).

[13] P. P. Gardner, C. Wilkinson, J. B. Forsyth, and B. M. Wanklyn, J. Phys. C **21**, 5653 (1988).

[14] C. Wilkinson, F. Sinclair, P. P. Gardner, J. B. Forsyth, and B. M. Wanklyn, J. Phys. C **14**, 1671 (1981).

[15] V. A. Sanina, L. M. Sapozhnikova, E. I. Golovenchits, and N. V. Morozov, Sov. Phys. Solid State **30**, 1736 (1988); E. I. Golovenchits, N. V. Morozov, V. A. Sanina, and L. M. Sapozhnikova, *ibid.* **34**, 56 (1992).

[16] M. T. Escote, A. M. L. da Silva, J. R. Matos, and R. F. Jardim, J. Solid State Chem. **151**, 298 (2000).

[17] F. F. Ferreira, E. Granado, W. Carvalho, Jr., S. W. Kycia, D. Bruno, and R. Droppa, Jr., J. Synchrotron Radiat. **13**, 46 (2006).

[18] E. I. Golovenchits, V. A. Sanina, and A. V. Babinskii, JETP **85**, 156 (1997).

[19] A. C. Larson and R. B. Von Dreele, Los Alamos National Laboratory Report No. LAUR 86–748, 1994 (unpublished).

[20] B. H. Toby, J. Appl. Crystallogr. **34**, 210 (2001).

[21] A. F. García-Flores, E. Granado, H. Martinho, R. R. Urbano, C. Rettori, E. I. Golovenchits, V. A. Sanina, S. B. Oseroff, S. Park, and S.-W. Cheong, Phys. Rev. B **73**, 104411 (2006).

[22] T. H. K. Barron and G. K. White, *Heat Capacity and Thermal Expansion at Low Temperatures* (Kluwer, Pordrecht/Plenum, New York, 1999).

[23] See, for example, U. Köbler, R. M. Mueller, P. J. Brown, R. R. Arons, and K. Fischer, J. Phys.: Condens. Matter **13**, 6835 (2001).

[24] T. A. Tyson, M. Deleon, S. Yoong, and S.-W. Cheong, Phys. Rev. B **75**, 174413 (2007).

[25] A. García-Flores and E. Granado (unpublished).

[26] N. E. Massa (private communication).

[27] A. Pimenov, A. A. Muckhin, V. Yu. Ivanov, V. D. Travkin, A. M. Balbashov, and A. Loidl, IEEE MICRO **2**, 97 (2006).

[28] A. B. Sushkov, R. V. Aguilar, S. Park, S.-W. Cheong, and H. D. Drew, Phys. Rev. Lett. **98**, 027202 (2007).

[29] R. Valdes Aguilar, A. B. Sushkov, S. Park, S.-W. Cheong, and H. D. Drew, Phys. Rev. B **74**, 184404 (2006).

[30] A. Pimenov, T. Rudolf, F. Mair, A. Loidl, A. A. Muckhin, and A. M. Balbashov, Phys. Rev. B **74**, 100403(R) (2006).